



Ni-doped MIL-53(Fe) nanoparticles for optimized doxycycline removal by using response surface methodology from aqueous solution

Weiping Xiong^{a,1}, Zhuotong Zeng^{b,1}, Xin Li^{a,1}, Guangming Zeng^{a,*}, Rong Xiao^{b,**}, Zhaohui Yang^a, Haiyin Xu^c, Hongbo Chen^d, Jiao Cao^a, Chengyun Zhou^a, Lei Qin^a

^a College of Environmental Science and Engineering, Hunan University and Key Laboratory of Environmental Biology and Pollution Control, Ministry of Education, Hunan University, Changsha, 410082, China

^b Department of Dermatology, Second Xiangya Hospital, Central South University, Changsha, 410011, Hunan, PR China

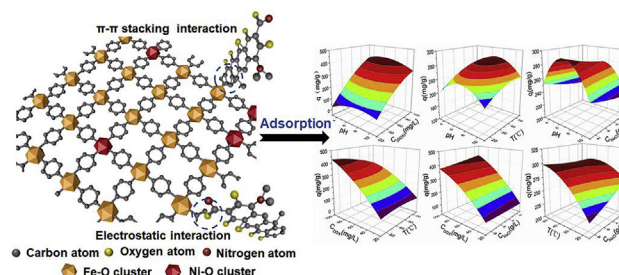
^c College of Environmental Science and Engineering, Central South University of Forestry and Technology, Changsha, 410004, China

^d College of Environment and Resources, Xiangtan University, Xiangtan, 411105, China

HIGHLIGHTS

- Ni-doped MIL-53(Fe) nanoparticles were applied to remove doxycycline for the first time.
- RSM was used to determine the optimum adsorption conditions for doxycycline removal.
- Electrostatic and π - π stacking interactions were possible adsorption mechanisms.
- Ni-doped MIL-53(Fe) was suggested as a reusable and efficient adsorbent.

GRAPHICAL ABSTRACT



ARTICLE INFO

Article history:

Received 23 February 2019

Received in revised form

30 April 2019

Accepted 22 May 2019

Available online 23 May 2019

Handling Editor: Chang-Ping Yu

Keywords:

Adsorption

Ni-doped MIL-53(Fe) nanoparticles

Doxycycline antibiotic

One-step solvothermal synthesis

Response surface quadratic model (RSM)

ABSTRACT

This study proposes a facile one-pot solvothermal method to prepare Ni-doped MIL-53(Fe) nanoparticles as high-performance adsorbents for doxycycline removal. The morphology and structure of the samples were characterized by scanning electron microscopy, transmission electron microscopy, X-ray diffraction, X-ray photoelectron spectroscopy, fourier transform infrared spectrum and thermogravimetric analysis. These results reveal that nickel was doped into MIL-53(Fe) successfully via a facile reaction, and the obtained Ni-doped MIL-53(Fe) nanoparticles showed excellent stability. The adsorption activities were evaluated in terms of the removal efficiencies of doxycycline (DOX) in aqueous solution. According to the response surface quadratic model (RSM), the optimal adsorption conditions were concentration of DOX 100 mg/L, temperature 35 °C, ionic strength 5 g/L and pH 7. The as-synthesized Ni-doped MIL-53(Fe) nanoparticles showed better adsorption capacity of 397.22 mg/g compared with other adsorbents. The investigation of adsorption mechanism demonstrated that the adsorption process was dominated by electrostatic and π - π stacking interactions. The Ni-doped MIL-53(Fe) nanoparticles with improved adsorption activities would have a great potential in DOX removal from aqueous environment.

© 2019 Elsevier Ltd. All rights reserved.

* Corresponding author. Hunan University, College of Environmental Science and Engineering, Changsha, 410082, PR China.

** Corresponding author.

E-mail addresses: zgming@hnu.edu.cn (G. Zeng), xiaorong65@csu.edu.cn (R. Xiao).

¹ These authors contribute equally to this article.

1. Introduction

As a typical antibiotic, doxycycline (DOX) is an emerging pollutant that has been widely used in human therapy of infectious

diseases and cultivation industry because of its specific antimicrobial property (Song et al., 2017; Chao et al., 2014). However, 30–90% of doxycycline-contained wastewater has been detected in the aqueous environment due to its lower bioavailability and good solubility, which led to increased antimicrobial resistance of microorganisms and impacted on human health (Zaidi et al., 2016; Liu et al., 2017). It is urgent need to find a solution to removal doxycycline pollution in the water.

In general, DOX removal methods include photodegradation (Zhou et al., 2018; Cao et al., 2018; Liu et al., 2019), Fenton-like (Cheng et al., 2019), electrochemistry (Xu et al., 2014, 2018; Zhang et al., 2015), ionic treatment (Mudgal et al., 2013; Chen et al., 2015; Wan et al., 2018), membrane separation (Homayoonfal and Mehrnia, 2014) and adsorption (Chao et al., 2014; Liu et al., 2017). Among them, some methods are limited in their application because of high energy consumption, low treatment efficiency and secondary pollution (Senta et al., 2011; Naeimi and Faghihian, 2017). Adsorption is considered as one of the most suitable methods in practical application because of its easy operation, low expense, nontoxicity and high efficiency (Cheng et al., 2018; Xiong et al., 2017; Xu et al., 2012a, 2012b; Tang et al., 2014; Long et al., 2011; Ren et al., 2018). Compared with graphene (Rostamian and Behnejad, 2018; Deng et al., 2013), carbon nanotubes (Zhang et al., 2016a; Gong et al., 2009), activated carbon (Fang et al., 2018), biochar (Lee et al., 2018; Tan et al., 2015; Liang et al., 2017; Wu et al., 2017), chitosan particles (Zhai et al., 2018) and clay mineral (Ayari, 2018), metal-organic frameworks (MOFs) are a class of porous crystal compounds with large porosity, easy tunability of their pore size, and easy to be modified, which enhances their adsorptive capacity by strengthening the interaction with the object molecules (Khan and Jhung, 2012; Stock and Biswas, 2011; Ahmed et al., 2014c; Xiong et al., 2018a). Therefore, we focus on the adsorption of DOX onto modified MOFs.

Over the past few decades, modified MOFs with transition metal ions have been reported in the literature. Montazerolghaem et al., 2016 synthesized two kind of Ni-MIL-101(Cr) and Cu-MIL-101(Cr) to improve the absorption capacity of CO₂ and adsorbent cyclability. However, they reported the BET surface area and pore volume of above modified MIL-101 (Cr) were less than MIL-101(Cr). Some researchers (Fu et al., 2016) reported Ni-doped NH₂-MIL-125(Ti) as a catalyst for photocatalytic oxidation of aromatic alcohols. They showed that the doping of Ni into MOFs could improve charge-separation and electron-transport to the enhanced photocatalytic activity. Li et al. (2012) found that Ni-doped MOF-5 not only exhibited larger surface areas and pores than MOF-5, but also improved its hydrostability. Besides, H₂ adsorptions of the Ni-doped MOF-5 could hold steady for four days. Si et al. (2011) reported a new strategy by doping Ammonia borane in Ni modified MIL-101 for hydrogen storage. This was the first report of such a big decrease (40 °C) in the pyrolysis temperature of Ammonia borane for AB/Ni@MIL-101. Ahmed et al. (2014a, b) loaded Lewis acid and CuCl into MIL-100(Fe) and MIL-100(Cr) for the adsorptive denitrogenation of model fossil fuels, respectively. Although the porosity of AlCl₃/MIL-100(Fe) and CuCl/MIL-100(Cr) were reduced, the adsorption of quinolone and nitrogen-containing compounds increased, respectively. To the best of our knowledge, the vast majority of work has been focused on the modification of MOFs for application of gas storage, photocatalytic degradation and fossil fuel purification, MOFs modified with transition metal ions as an adsorbent for contaminant removal are relatively scarce in aqueous environment.

MIL-53(Fe) as one of the most intensively investigated materials with high chemical stability and multifunctional property has been researched for its potential applications (Naeimi and Faghihian, 2017). In this study, Ni-doped MIL-53(Fe) was synthesized for

adsorption removal of doxycycline in aqueous solutions. What's more, response surface methodology (RSM) as a popular optimization method was used to assess the relationship between a set of parameters, including DOX concentration, temperature, pH and ionic strength, and the observed response of adsorption removal of DOX. In addition, adsorption kinetics, isotherms, thermodynamics and adsorption mechanisms were investigated in detail. This study provides valuable information into the design of modified MOFs adsorbents for antibiotic removal in aqueous environment.

2. Experimental section

2.1. Chemicals and syntheses of adsorbents

Chemical reagents, Nickel (II) chloride hexahydrate (NiCl₂·6H₂O, 98%), iron (III) chloride hexahydrate (FeCl₃·6H₂O, 99%), N, N-dimethylformamide (DMF, 99.5%), ethanol (99.5%) and 1, 4-benzenedicarboxylic acid (1,4-BDC) (99%) were purchased from Sinopharm Chemical Reagent Co., Ltd. (Shanghai, China). Doxycycline hydrochloride (DOX) was obtained from Bomei biotechnology Co., Ltd (Hefei, China). All the chemical reagents were analytical grade and used without further purification. The ultra-pure water (resistivity of 18.25 MΩ cm⁻¹) was used throughout the whole experiments.

Ni-MIL-53(Fe) was prepared by a one-step solvothermal method. In a typical procedure, FeCl₃·6H₂O, 1, 4-BDC and DMF solution with the molar ratio of 1:1:280 were mixed. Proper amount of NiCl₂·6H₂O (NiCl₂·6H₂O and FeCl₃·6H₂O with the molar ratio of 1:1, 1:3, 1:5, 1:7) was added in above mixture and then stirred for 2 h at room temperature. The resulting solution was transferred into a 100 mL Teflon-lined bomb and heated at 170 °C for 24 h. The powder was collected by centrifugation, washed with DMF and ethanol, and dried under vacuum at 100 °C for 12 h. The obtained powder was named as Ni-MIL-53(Fe)-X (X = 1, 3, 5 and 7, which represents for the NiCl₂·6H₂O: FeCl₃·6H₂O mole ratio). For comparison, the MIL-53(Fe) was synthesized according to the same method.

2.2. Characterization

The morphology of Ni-MIL-53(Fe)-1 was examined via the scanning electron microscope (SEM, Carl Zeiss, EVO-MA10) and transmission electron microscope (TEM, JEOL JEM-2100F). The crystal phase of Ni-MIL-53(Fe)-X was analyzed by an X-ray diffractometer (XRD; Bruker, Germany). The surface composition of Ni-MIL-53(Fe)-1 was studied by an X-ray photoelectron spectrum (XPS) (Thermo Fisher Scientific-ESCALAB 250Xi, USA). The thermostability of materials was measured by a Mettler TGA/SDT Q600 analyzer. The Fourier transform infrared spectrum (FT-IR) measurements were obtained from a Nicolet 5700 Spectrometer in KBr pellet at room temperature (Nicolet, USA).

2.3. Adsorption experiments

The stock solution for DOX (150 mg/L) was prepared by dissolving 0.15 g of C₂₂H₂₄N₂O₈ in water and diluted to different concentrations of solutions (5–150 mg/L). All of the adsorption experiments were carried out in 50 mL conical flasks containing 50 mL of DOX solution of desired concentrations. Before the experiment, the adsorbents of Ni-MIL-53(Fe)-X were dried at 100 °C for 8 h in a vacuum oven and used for the adsorption of DOX from water. The adsorbent (10 mg) was added to each solution (50 mL) in a conical flask and the mixture was stirred at a constant speed (200 rpm) at different temperatures. The solutions were then centrifuged at 5000 rpm for 5 min and filtered by 0.45 μm PVDF

disposable filters, and the concentration of pretreated solutions was determined by UV spectrophotometer (at 346 nm, UV-2700, SHIMADZU, Japan). The detailed equations and models, such as kinetics, isotherm and thermodynamic models were shown in Table S1. The experimental factors, including pH, ionic strength and humic acid, were taken into account. The recyclability of Ni-MIL-53(Fe)-1 for DOX was evaluated by washing with water/acetone and dried in a vacuum oven.

2.4. Doxycycline removal using a RSM experimental design model

The central composite design model (CCD) was employed to evaluate the factors which made sense on the adsorption capacity of doxycycline. In this design, four factors were the pH (x_1), concentration of doxycycline (x_2), temperature (x_3) and ionic strength (x_4), each at five levels (-2, -1, 0, 1, 2). The response variable (y) that represented adsorption capacity was fitted by a second-order model in the form of quadratic polynomial equation (Yang et al., 2009):

$$y = \beta_0 + \sum_{i=1}^m \beta_i x_i + \sum_{i < j} \beta_{ij} x_i x_j + \sum_{i=1}^m \beta_{ii} x_i^2 \quad (1)$$

where y is adsorption capacity of doxycycline, β_0 is the model coefficient, β_i is the linear coefficient, β_{ij} is the interaction coefficient, β_{ii} is the quadratic coefficient, x_i , x_j are the independent variables which determine y , m is the number of independent variables. Response surface methodology (RSM) experiments were analyzed using the statistic software (version, 8.0.6).

3. Results and discussion

3.1. Characterization of the adsorbents

The morphology and compositions of Ni-MIL-53(Fe)-1 were determined by SEM with EDS analysis in Fig. 1. It was observed that the Ni-MIL-53(Fe)-1 was crystallized in spindle structures (Fig. 1a). Meanwhile, the EDS mappings for the prepared adsorbent were also shown in Fig. 1c–g. The elements of C, Fe, O and Ni were observed on the surface. Subsequently, the structures of the testing products were characterized by TEM (Fig. 1b). Based on the obtained results presented in Fig. 1b, obvious black spots can easily be identified, suggesting that the presence of the oxidative Ni in the nanoparticles.

The structures of virgin MIL-53(Fe) and Ni-MIL-53(Fe)-X were characterized with XRD. As shown in Fig. S1a, the XRD pattern of the MIL-53(Fe) was analogous to the reported in previous literature, confirming the successful synthesis of MIL-53(Fe) (Gao et al., 2017). In order to give a better comparison, the XRD patterns of Ni-MIL-53(Fe)-1, Ni-MIL-53(Fe)-3, Ni-MIL-53(Fe)-5 and Ni-MIL-53(Fe)-7 were included. The virgin MIL-53(Fe) and Ni-doped MIL-53(Fe) exhibited good crystallinity, which demonstrated that the structure of MIL-53(Fe) was remained after Ni-doped. However, the characteristic peak of nickel was more and more obvious with the increase of nickel doping, and made no difference to the diffraction peak positions of MIL-53(Fe), these results indicated the Ni-doped modification did not influence the crystallinity of MIL-53(Fe).

For a more in-depth study, The FT-IR spectroscopy of the virgin and Ni-doped MIL-53(Fe) was presented in Fig. S1b. The five samples exhibited similar spectra because of the extremely low nickel content, further confirming the isostructure (Li et al., 2012). It is obvious that characteristic peaks of MIL-53(Fe) were observed. For instance, the band at 538 cm^{-1} was assigned to Fe-O vibration. Bands at 1390 and 1540 cm^{-1} were attributed to C-O vibration, and

the band at 1650 cm^{-1} was assigned to C=O vibration (Xiong et al., 2018b). The MIL-53(Fe) framework kept integrated after Ni-doped, which was in consistent with the results of XRD analysis. The TGA curves of virgin and Ni-doped MIL-53(Fe) displayed two main steps of weight loss in Fig. S2. The first step could be attributed to the loss of solvents from the framework. The second step was due to the decomposition of structural organic ligands. Compared to that of virgin MIL-53(Fe), the second step of weight loss occurred faster. This phenomenon indicated that the doping of nickel played an important role in keeping a good structure.

X-ray photoelectron spectroscopy (XPS) was applied to confirm the surface chemical state of Ni-MIL-53(Fe)-1. As shown in Fig. 2, the XPS survey spectrum of Ni-MIL-53(Fe)-1 was composed of Ni, Fe, C and O elements, which was consistent with analysis of elemental mappings in Fig. 1c–g. As presented in Fig. 2b, the C 1s peak of Ni-MIL-53(Fe)-1 could be fitted into two peaks at 284.85 eV and 288.71 eV, which was mainly attributed to benzoic rings (C=C) and the carboxylate groups on the H₂BDC linkers (C=O), respectively (Tam et al., 2005). Fig. 2c showed that the O 1s peak was fitted into two peaks at 531.86 and 532.38 eV, which was attributed to the carboxylate groups and the Fe-O bonds and Ni-O bonds of Ni-MIL-53(Fe)-1 (Liang et al., 2015). In the XPS Fe 2p spectrum (Fig. 2d), the appearance of two peaks at 725.83 eV and 712.87 eV were attributed to Fe 2p_{1/2} and Fe 2p_{3/2}, which were characteristic of ferric iron in Ni-MIL-53(Fe)-1 (Du et al., 2011). The Ni 2p spectrum was shown in Fig. 2e, the two binding energies of 855.26 eV and 874.32 eV were ascribed to Ni 2p_{3/2} and Ni 2p_{1/2} respectively, indicating that oxidative Ni existed in Ni-MIL-53(Fe)-1 (Fu et al., 2016).

3.2. Adsorption studies

Different mole ratios of Ni-MIL-53(Fe)-X presented different adsorption capacities to DOX. As shown in Fig. S3, the adsorption capacity of Ni-MIL-53(Fe)-1 was much greater than MIL-53(Fe), Ni-MIL-53(Fe)-3, Ni-MIL-53(Fe)-5 and Ni-MIL-53(Fe)-7, indicating that the adsorption capacity of adsorbents enhanced with the increase of nickel doping. Hence, Ni-MIL-53(Fe)-1 was used as the best adsorbent throughout the research.

3.2.1. Adsorption kinetics and isotherms

The adsorption experiments of DOX from aqueous solutions by Ni-MIL-53(Fe)-1 were conducted at different temperatures (15, 35 and 55 °C) and concentrations of pollutants (5, 10, 20, 40, 60, 80, 100, 120 and 150 mg/L). The experimental results analyzed by pseudo first-order and pseudo second-order models were shown in Fig. 3 and Table S2. All correlation coefficients (R^2) of pseudo first-order equation were much higher. Compared to pseudo first-order model, the pseudo second-order model exhibited a better fitting with the experimental results, which demonstrated that the chemical adsorption might be the major limiting step in the adsorption of DOX.

As shown in Fig. S4, the equilibrium adsorption capacity of DOX on Ni-MIL-53(Fe)-1 increased with the enhance temperature and initial DOX concentration. Langmuir and Freundlich models were used to analyze adsorption mechanism, and all obtained results were presented in Fig. 4 and Table S3. In this research, separation factor (R_L) and heterogeneity factor ($1/n$) were all below 1, which indicated that the favorable adsorption between DOX and Ni-MIL-53(Fe)-1 (Wang et al., 2017; Tang et al., 2018). It was evident that the correlation coefficients (R^2) of Langmuir model were much higher than that of Freundlich isotherm model, indicating that monolayer chemical adsorption played a major role. In addition, the maximum adsorption capacity of Ni-MIL-53(Fe)-1 for DOX was reaching to 684.32 mg/g at 55 °C, which was much higher than other adsorbents in Table S4.

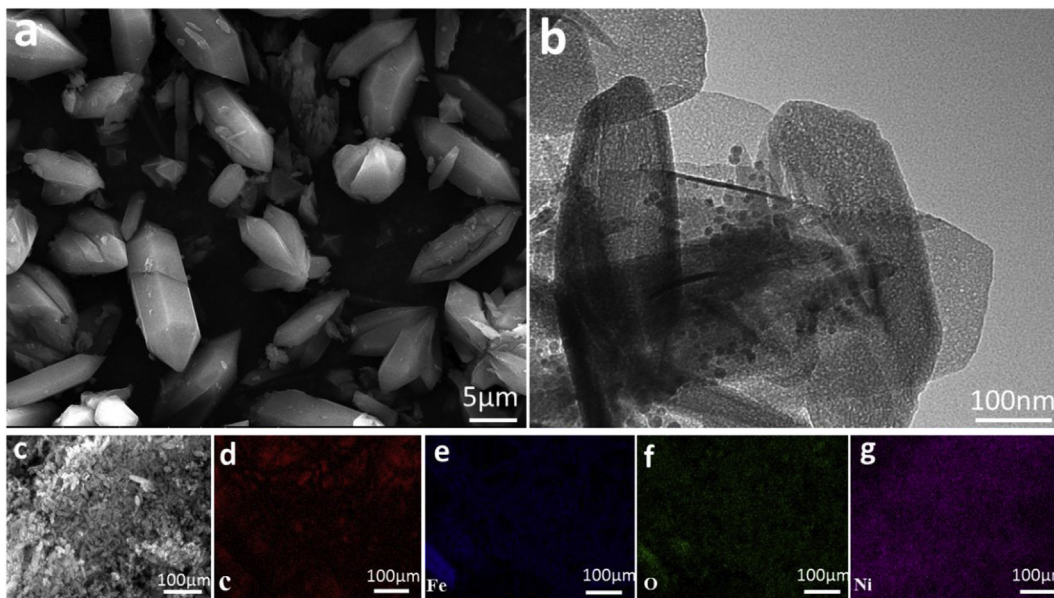


Fig. 1. The SEM images of Ni-MIL-53(Fe)-1 (a); the TEM images of Ni-MIL-53(Fe)-1 (b); and corresponding elemental maps of Ni-MIL-53(Fe)-1 (c–g).

3.2.2. Thermodynamic analysis

The experimental data were fitted by Gibbs-Helmholtz equation, and the results of thermodynamic analysis were shown in Table S5. The negative values of ΔG at different experimental temperature proved that DOX adsorption on Ni-MIL-53(Fe)-1 was spontaneous and endothermic. Furthermore, the ΔG value decreased from -2.289 to -3.371 (kJ/mol) with the increase of temperature, revealing that the adsorption performance was more favorable at a relatively higher temperature. The positive value of ΔH indicated that adsorption was an endothermic process, which was consistent with the results of previous adsorption isotherm. The positive value of ΔS manifested that the affinity and the randomness at the adsorbent-adsorbate interface increased.

3.2.3. The effect of ionic strength, humic acid and pH

Salts and humic acid exist in most of actual waters. In this study, a typical cation Na^+ (1, 3, 5, 7 and 9 g/L) and HA (10, 20, 30, 40 and 50 mg/L) were set separately inside solutions to investigate the competitive effect on the adsorption of DOX on Ni-MIL-53(Fe)-1. As shown in Fig. S5a, NaCl obviously decreased adsorption capacity of DOX. The higher concentration of sodion, the less DOX was adsorbed by Ni-MIL-53(Fe)-1. This is because Na^+ may compete with DOX for the same active site of Ni-MIL-53(Fe)-1 via donor-acceptor interaction.

was shown in Fig. S6. As can be seen, the pH ranging from 2.0 to 11.0 was a major factor that affected the adsorption capacity of DOX. As pH increased from 2.0 to 4.0, the adsorption capacity of DOX increased rapidly from 48.27 to 86.43 mg/g. However, when the pH further increased from 4.0 to 10.0, the adsorption capacity of DOX decreased slightly from 86.43 to 79.99 mg/g. When the pH was greater than 10.0, the adsorption decreased quickly from 79.99 to 72.60 mg/g.

3.3. Experimental results of response surface methodology

Four key parameters affecting adsorption capacity of DOX on Ni-MIL-53(Fe)-1 were selected as variables of the design matrix in Table S6. The response variable, such as adsorption capacity, acquired from 30 groups of experiments including parallel control groups were shown in Table 1.

3.3.1. Analysis of variance (ANOVA)

The adsorption capacity of DOX in the experimental results ranged between 92.19 mg/g and 397.22 mg/g. The quadratic polynomial equation between adsorption capacity (y) and four variables (x_1-x_4) was used for regression analysis, as follows:

$$Y = -262.31 + 52.16X_1 + 6.16X_2 + 3.33X_3 - 1.06X_4 - 0.08X_1X_2 - 0.26X_1X_3 - 0.13X_1X_4 + 0.05X_2X_3 - 0.12X_2X_4 + 0.19X_3X_4 - 2.78X_1^2 - 0.02X_2^2 - 0.07X_3^2 + 0.11X_4^2 \quad (2)$$

The effect of humic acid on the DOX sorption on Ni-MIL-53(Fe)-1 was displayed in Fig. S5b. The adsorption capacity of Ni-MIL-53(Fe)-1 only decreased about 10% with high HA concentration (50 mg/L), indicating that humic acid has little effect on adsorption capacity. The little influence caused by humic acid could be interpreted by competition for adsorption sites on Ni-MIL-53(Fe)-1.

The influence of pH on adsorption of DOX on Ni-MIL-53(Fe)-1

The analysis of variance (ANOVA) for response surface quadratic model was shown in Table 2. The p-value of the model was less than 0.0001 and determination coefficient R^2 reached 0.9991, indicating that the second order equation model fitted well. The F values of X_1 ($P < 0.0001$), X_2 ($P < 0.0001$), X_3 ($P < 0.0001$), X_4 ($P < 0.0001$), X_1X_2 ($P < 0.0001$), X_1X_3 ($P < 0.0001$), X_2X_3 ($P < 0.0001$), X_2X_4 ($P < 0.0001$), X_3X_4 ($P < 0.0001$), X_1^2 ($P < 0.0001$), X_2^2 ($P < 0.0001$)

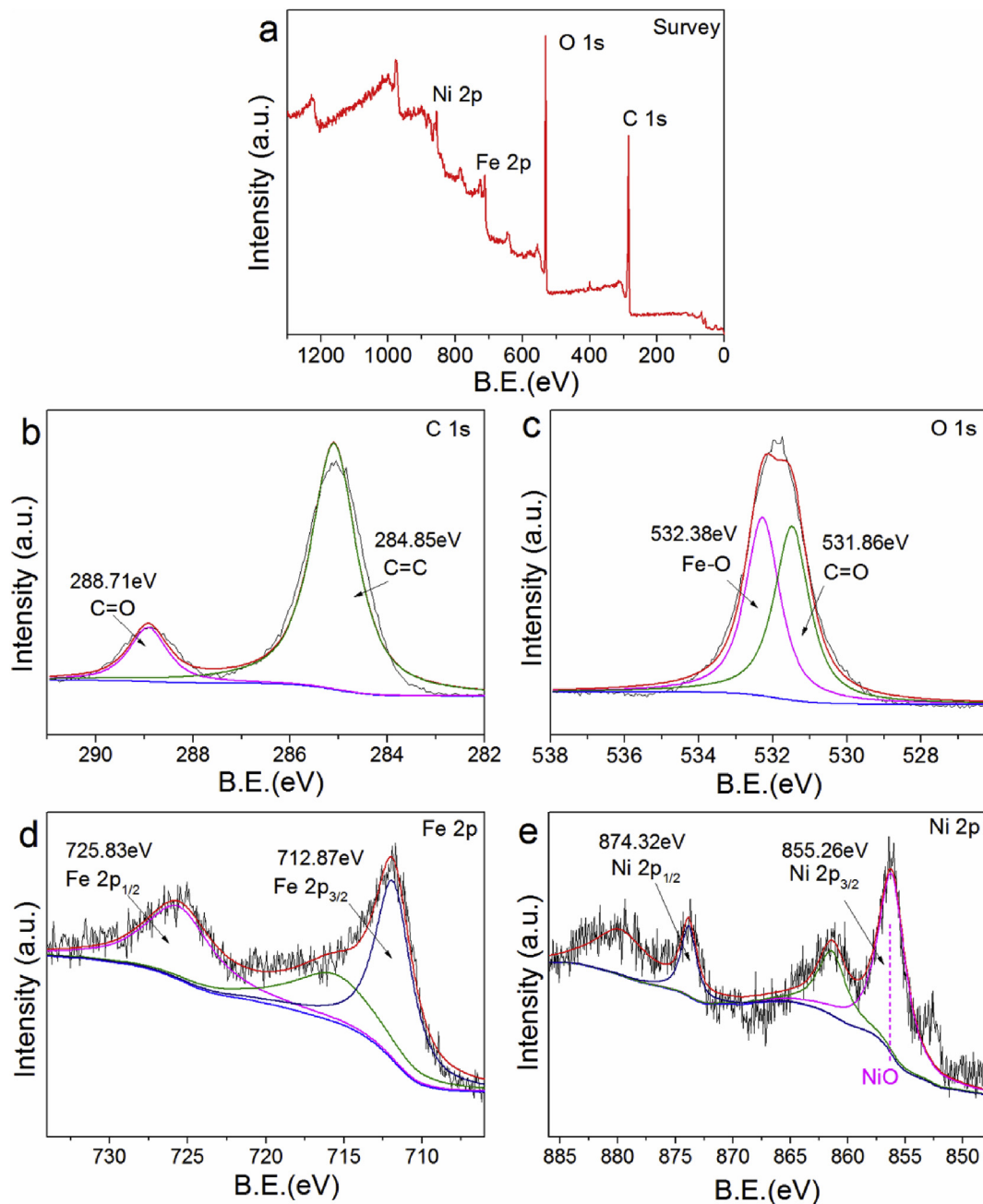


Fig. 2. The XPS spectra of Ni-MIL-53(Fe)-1: (a) the full XPS spectra of Ni-MIL-53(Fe)-1, (b) C 1s, (c) O 1s, (d) Fe 2p and (e) Ni 2p.

and X_3^2 ($P < 0.0001$) were statistically significant, Nevertheless, X_1X_4 ($P = 0.3468$) and X_4^2 ($P = 0.3165$) were not significant. According to the response surface quadratic model, the effect of each parameter on adsorption capacity of DOX on Ni-MIL-53(Fe)-1 was: concentration of DOX > temperature > pH > ionic strength. The optimal adsorption conditions were concentration of DOX 100 mg/L, temperature 35 °C, ionic strength 5 g/L and pH 7. The adsorption capacity of DOX reached 397.22 mg/g under the optimal adsorption conditions.

3.3.2. Effects of interaction on the adsorption of DOX

The response surfaces for the interaction between the variables on adsorption of DOX are displayed in Fig. 5a–f, respectively. As

shown in Fig. 5a, the change of adsorption capacity with pH and concentration of DOX, while temperature and ionic strength were kept at central level. The figure of the curve indicated that pH has visible quadratic effect on the adsorption of DOX, which was consistent with the previous study considering pH value only. Moreover, the adsorption capacity increased with the concentration of DOX. According to Fig. 5b, adsorption of DOX increased considerably when the temperature increased, no matter what happened to pH. This phenomenon indicated that the adsorption was an endothermic process. Fig. 5c showed that, when the temperature and concentration of DOX were at central level, the adsorption of DOX decreased slightly when the ionic strength increased, which indicated that there was competition for

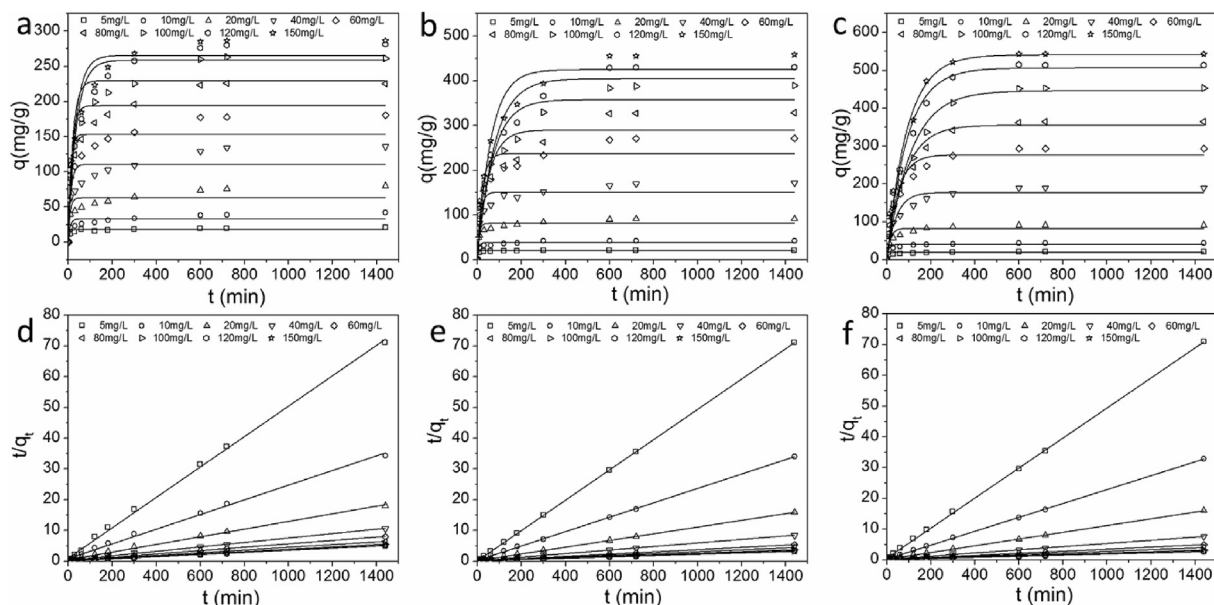


Fig. 3. The pseudo-first order plots for DOX (a, 15 °C; b, 35 °C; c, 55 °C) adsorption; the pseudo-second order plots for DOX (d, 15 °C; e, 35 °C; f, 55 °C) adsorption. Reaction conditions: adsorbent loading = 0.2 g/L; initial pH = 7.

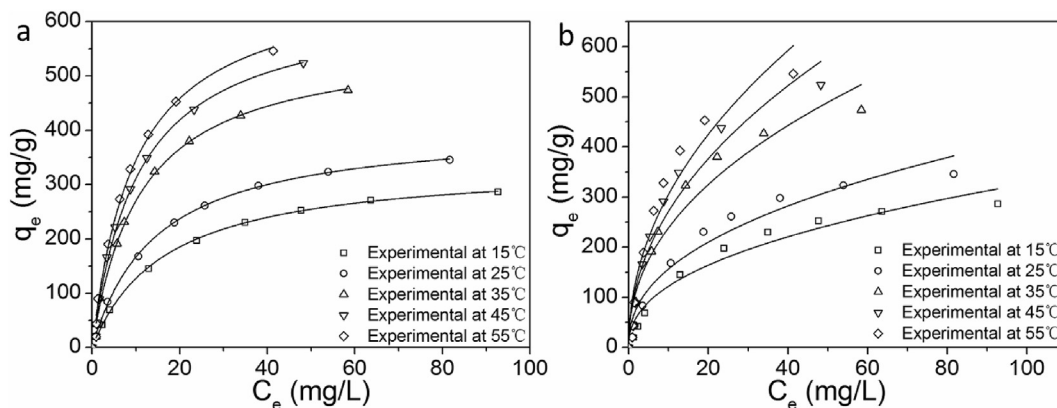


Fig. 4. The Langmuir isotherm model for DOX (a) adsorption; the Freundlich isotherm model for DOX (b) adsorption. Reaction conditions: adsorbent loading = 0.2 g/L; initial pH = 7.

adsorption sites at different pH values (Lin et al., 2018). Fig. 5d and e indicated that the influence of concentration of DOX on its adsorption was greater than that of temperature and ionic strength, and this was in accordance with above-mentioned analysis of variance. In addition, the effect of temperature on adsorption was greater than that of ionic strength (Fig. 5f).

3.4. Mechanisms for DOX adsorption

It can be seen from the above single-factor analysis and multi-factor analysis that pH has a great influence on adsorption. Consequently, it is important to further study the adsorption mechanism. The dissociation constants (pKa) of DOX were 3.3, 7.7 and 9.7, indicating that DOX has positive charge at $\text{pH} < 3.3$, neutral charge at $3.3 < \text{pH} < 7.7$, negative charge at $\text{pH} > 7.7$ (Zhang et al., 2016b). As shown in Fig. S6, with the $\text{pH} < 4.0$ or $\text{pH} > 10.0$, the adsorption capacity of DOX decreased obviously, demonstrating that electrostatic interactions existed between the DOX and Ni-MIL-53(Fe)-1 and became the main factor affecting adsorption. As

pH increased from 4.0 to 10.0, DOX existed mainly in the form of zwitterions (Chao et al., 2014). Electrostatic adsorption and electrostatic repulsion were difficult to play a role in this case. And π - π stacking interactions acted as a dominant driving force, due to the structure of aromatic rings existing in both DOX and Ni-MIL-53(Fe)-1. In conclusion, electrostatic and π - π stacking interactions were the main mechanisms.

3.5. Reusability of Ni-MIL-53(Fe)-1

Reusability as an important factor should be taken into consideration for commercial applications. Regeneration of Ni-MIL-53(Fe)-1 was evaluated after washing the used adsorbents with methanol and drying them at 100 °C in a vacuum oven. As displayed in Fig. S7, the adsorption capacity of DOX had no significant decrease after the fifth recycling cycles. The results demonstrated that the synthesized Ni-MIL-53(Fe)-1 is reusable and thus can meet the requirements of a large number of water treatment applications.

Table 1
Experimental design matrix for removal of DOX.

Run	x_1	x_2	x_3	x_4	y	
					Observed ^a	Predicted ^b
1	9.00	40.00	45.00	3.00	168.30	168.16
2	7.00	60.00	35.00	5.00	283.33	283.21
3	7.00	60.00	55.00	5.00	275.70	273.99
4	7.00	20.00	35.00	5.00	92.19	90.53
5	5.00	80.00	25.00	3.00	328.47	326.10
6	5.00	80.00	45.00	7.00	362.10	359.54
7	5.00	80.00	25.00	7.00	304.13	304.55
8	7.00	60.00	35.00	5.00	282.86	283.21
9	5.00	40.00	25.00	3.00	176.41	176.16
10	7.00	60.00	35.00	5.00	283.33	283.21
11	5.00	40.00	25.00	7.00	174.51	173.57
12	11.00	60.00	35.00	5.00	235.62	233.56
13	7.00	60.00	35.00	9.00	280.95	279.40
14	9.00	80.00	25.00	7.00	300.32	302.17
15	7.00	60.00	35.00	5.00	282.86	283.21
16	9.00	80.00	25.00	3.00	328.47	325.86
17	7.00	60.00	35.00	1.00	289.30	290.53
18	9.00	40.00	25.00	3.00	186.20	188.80
19	7.00	60.00	35.00	5.00	283.33	283.21
20	5.00	80.00	45.00	3.00	364.49	365.94
21	7.00	60.00	35.00	5.00	283.57	283.21
22	7.00	60.00	15.00	5.00	238.25	239.64
23	9.00	40.00	25.00	7.00	185.24	184.07
24	7.00	100.00	35.00	5.00	397.22	398.53
25	9.00	80.00	45.00	3.00	344.21	345.18
26	5.00	40.00	45.00	7.00	185.72	188.60
27	3.00	60.00	35.00	5.00	242.06	243.81
28	9.00	80.00	45.00	7.00	336.10	336.64
29	5.00	40.00	45.00	3.00	177.85	176.04
30	9.00	40.00	45.00	7.00	176.18	178.58

^a Experimental values of response.

^b Predicted values of response by RSM.

Table 2
ANOVA for response surface quadratic model.

Source	Sum of squares	Df	Mean square	F Value	p-value Prob > F
Model	153218.03	14	10944.15	2239.75	<0.0001
X_1	185.89	1	185.89	38.04	<0.0001
X_2	132295.41	1	132295.41	4518.17	<0.0001
X_3	1770.00	1	1770.00	362.24	<0.0001
X_4	157.83	1	157.83	32.30	<0.0001
$X_1 X_2$	165.94	1	165.94	33.96	<0.0001
$X_1 X_3$	420.88	1	420.88	86.13	<0.0001
$X_1 X_4$	4.61	1	4.61	0.94	0.3468
$X_2 X_3$	1596.57	1	1596.57	326.74	<0.0001
$X_2 X_4$	359.66	1	359.66	73.61	<0.0001
$X_3 X_4$	229.46	1	229.46	46.96	<0.0001
X_1^2	3399.18	1	3399.18	695.65	<0.0001
X_2^2	2565.45	1	2565.45	525.03	<0.0001
X_3^2	1194.74	1	1194.74	244.51	<0.0001
X_4^2	5.25	1	5.25	1.07	0.3165
Residual	73.29	15	4.89		
Lack of Fit	72.87	10	7.29	85.37	<0.0001
Pure Error	0.43	5	0.09		
Cor Total	143291.33	29			
R^2	0.9991				

4. Conclusion

In conclusion, Ni-MIL-53(Fe) nanoparticles have been prepared via a solvothermal process, characterized and used as an adsorbent for adsorption in DOX from aqueous solutions. The optimized Ni-MIL-53(Fe)-1 exhibited much higher adsorption capacity of DOX than other adsorbents reported in the literature. The

thermodynamic parameters indicated that the adsorption DOX adsorption on Ni-MIL-53(Fe)-1 was spontaneous and endothermic. According to the response surface quadratic model, the effect of each parameter on adsorption capacity of DOX on Ni-MIL-53(Fe)-1 was: concentration of DOX > temperature > pH > ionic strength. Electrostatic and π - π stacking interactions were the main mechanisms for DOX adsorption onto Ni-MIL-53(Fe)-1. Considering this

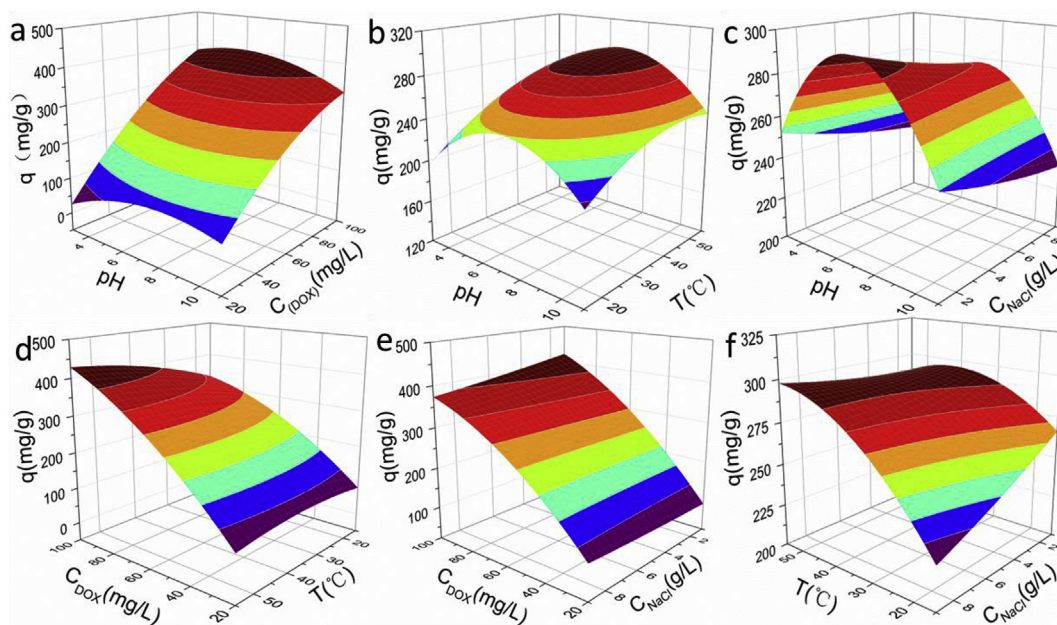


Fig. 5. Surface graphs for the effect of different variables on DOX removal: (a) C(DOX)-pH, (b) T-pH, (c) C(NaCl)-pH, (d) C(DOX)-T, (e) C(DOX)-C(NaCl) and (f) T-C(NaCl).

simple synthetic strategy, high absorbability and good recyclability, the Ni-MIL-53(Fe)-1 is a promising and practical adsorbent for removal of DOX in aqueous solutions.

Acknowledgement

The study was financially supported by the National Natural Science Foundation of China (81773333, 51521006, 51378190, 51578223 and 51608464), the Program for Changjiang Scholars and Innovative Research Team in University (IRT-13R17), the Natural Science Foundation of Hunan Province (2017JJ3291), the Research Foundation of Education Bureau of Hunan Province (17B256), the Key Research and Development Program of Hunan Province (2017SK2242).

Appendix A. Supplementary data

Supplementary data to this article can be found online at <https://doi.org/10.1016/j.chemosphere.2019.05.184>.

References

- Ahmed, I., Jun, J.W., Jung, B.K., Jhung, S.H., 2014. Adsorptive denitrogenation of model fossil fuels with Lewis acid-loaded metal-organic frameworks (MOFs). *Chem. Eng. J.* 255, 623–629.
- Ahmed, I., Jhung, S.H., 2014b. Adsorptive denitrogenation of model fuel with CuCl-loaded metal-organic frameworks (MOFs). *Chem. Eng. J.* 251, 35–42.
- Ahmed, I., Jhung, S.H., 2014c. Composites of metal-organic frameworks: preparation and application in adsorption. *Mater. Today* 17, 136–146.
- Ayari, F., 2018. Hybrid clay mineral for anionic dye removal and textile effluent treatment. *Nanotechnol. Sustain. Water Res.* 407–459.
- Cao, J., Yang, Z.H., Xiong, W.P., Zhou, Y.Y., Peng, Y.Y., Li, X., Zhou, C.Y., Xu, R., Zhang, Y.R., 2018. One-step synthesis of Co-doped UiO-66 nanoparticle with enhanced removal efficiency of tetracycline: simultaneous adsorption and photocatalysis. *Chem. Eng. J.* 353, 126–137.
- Cheng, M., Liu, Y., Huang, D.L., Lai, C., Zeng, G.M., Huang, J.H., Liu, Z.F., Zhang, C., Zhou, C.Y., Qin, L., Xiong, W.P., Yi, H., Yang, Y., 2019. Prussian blue analogue derived magnetic Cu-Fe oxide as a recyclable photo-Fenton catalyst for the efficient removal of sulfamethazine at near neutral pH values. *Chem. Eng. J.* 362, 865–876.
- Cheng, M., Zeng, G., Huang, D., Lai, C., Liu, Y., Zhang, C., Wang, R., Qin, L., Xue, W., Song, B., Ye, S., Yi, H., 2018. High adsorption of methylene blue by salicylic acid-methanol modified steel converter slag and evaluation of its mechanism. *J. Colloid Interface Sci.* 515, 232–239.

- Chao, Y., Zhu, W., Wu, X., Hou, F., Xun, S., Wu, P., Ji, H., Xu, H., Li, H., 2014. Application of graphene-like layered molybdenum disulfide and its excellent adsorption behavior for doxycycline antibiotic. *Chem. Eng. J.* 243, 60–67.
- Chen, M., Xu, P., Zeng, G., Yang, C., Huang, D., Zhang, J., 2015. Bioremediation of soils contaminated with polycyclic aromatic hydrocarbons, petroleum, pesticides, chlorophenols and heavy metals by composting: applications, microbes and future research needs. *Biotechnol. Adv.* 33, 745–755.
- Deng, J.H., Zhang, X.R., Zeng, G.M., Gong, J.L., Niu, Q.Y., Liang, J., 2013. Simultaneous removal of Cd (II) and ionic dyes from aqueous solution using magnetic graphene oxide nanocomposite as an adsorbent. *Chem. Eng. J.* 226, 189–200.
- Du, J.J., Yuan, Y.P., Sun, J.X., Peng, F.M., Jiang, X., Qiu, L.G., Xie, A.J., Shen, Y.H., Zhu, J.F., 2011. New photocatalysts based on MIL-53 metal-organic frameworks for the decolorization of methylene blue dye. *J. Hazard Mater.* 190, 945–951.
- Fang, R., Huang, H., Ji, J., He, M., Peng, Q., Zhan, Y., Leung, D.Y., 2018. Efficient MnOx supported on coconut shell activated carbon for catalytic oxidation of indoor formaldehyde at room temperature. *Chem. Eng. J.* 334, 2050–2057.
- Fu, Y., Sun, L., Yang, H., Xu, L., Zhang, F., Zhu, W., 2016. Visible-light-induced aerobic photocatalytic oxidation of aromatic alcohols to aldehydes over Ni-doped NH₂-MIL-125 (Ti). *Appl. Catal. B Environ.* 187, 212–217.
- Gao, Y., Li, S., Li, Y., Yao, L., Zhang, H., 2017. Accelerated photocatalytic degradation of organic pollutant over metal-organic framework MIL-53 (Fe) under visible LED light mediated by persulfate. *Appl. Catal. B Environ.* 202, 165–174.
- Gong, J.L., Wang, B., Zeng, G.M., Yang, C.P., Niu, C.G., Niu, Q.Y., Liang, Y., 2009. Removal of cationic dyes from aqueous solution using magnetic multi-wall carbon nanotube nanocomposite as adsorbent. *J. Hazard Mater.* 164, 1517–1522.
- Homayoonfal, M., Mehrnia, M.R., 2014. Amoxicillin separation from pharmaceutical solution by pH sensitive nanofiltration membranes. *Separ. Purif. Technol.* 130, 74–83.
- Khan, N.A., Jhung, S.H., 2012. Low-temperature loading of Cu⁺ species over porous metal-organic frameworks (MOFs) and adsorptive desulfurization with Cu⁺-loaded MOFs. *J. Hazard Mater.* 237, 180–185.
- Liang, R., Jing, F., Shen, L., Qin, N., Wu, L., 2015. MIL-53 (Fe) as a highly efficient bifunctional photocatalyst for the simultaneous reduction of Cr (VI) and oxidation of dyes. *J. Hazard Mater.* 287, 364–372.
- Liu, Y., Liu, Z.F., Huang, D.L., Cheng, M., Zeng, G.M., Lai, C., Zhang, C., Zhou, Chengyun, Wang, W.J., Jiang, D.N., Wang, H., Shao, B.B., 2019. Metal or metal-containing nanoparticle@MOF nanocomposites as a promising type of photocatalyst. *Coord. Chem. Rev.* 388, 63–78.
- Liu, S., Xu, W.H., Liu, Y.G., Tan, X.F., Zeng, G.M., Li, X., Liang, J., Zhou, Z., Yan, Z.L., Cai, X.X., 2017. Facile synthesis of Cu (II) impregnated biochar with enhanced adsorption activity for the removal of doxycycline hydrochloride from water. *Sci. Total Environ.* 592, 546–553.
- Lin, J., Su, B., Sun, M., Chen, B., Chen, Z., 2018. Biosynthesized iron oxide nanoparticles used for optimized removal of cadmium with response surface methodology. *Sci. Total Environ.* 627, 314–321.
- Long, F., Gong, J.L., Zeng, G.M., Chen, L., Wang, X.Y., Deng, J.H., Niu, Q.Y., Zhang, H.Y., Zhang, X.R., 2011. Removal of phosphate from aqueous solution by magnetic Fe-Zr binary oxide. *Chem. Eng. J.* 171, 448–455.
- Lee, D.J., Cheng, Y.L., Wong, R.J., Wang, X.D., 2018. Adsorption removal of natural organic matters in waters using biochar. *Bioresour. Technol.* 260, 413–416.

- Liang, J., Yang, Z., Tang, L., Zeng, G., Yu, M., Li, X., Wu, H., Qian, Y., Li, X., Luo, Y., 2017. Changes in heavy metal mobility and availability from contaminated wetland soil remediated with combined biochar-compost. *Chemosphere* 181, 281–288.
- Li, H., Shi, W., Zhao, K., Li, H., Bing, Y., Cheng, P., 2012. Enhanced hydrostability in Ni-doped MOF-5. *Inorg. Chem.* 51, 9200–9207.
- Mudgal, S., Toni, A.De, Lockwood, S., Salès, K., Backhaus, T., Sorensen, B.H., 2013. Study on the Environmental Risks of Medicinal Products. Execu. Agency Health Consum, p. 310.
- Montazerolghaem, M., Aghamiri, S.F., Tangestaninejad, S., Talaie, M.R., 2016. A metal–organic framework MIL-101 doped with metal nanoparticles (Ni & Cu) and its effect on CO₂ adsorption properties. *RSC Adv.* 6, 632–640.
- Naeimi, S., Faghihian, H., 2017. Application of novel metal organic framework, MIL-53 (Fe) and its magnetic hybrid: for removal of pharmaceutical pollutant, doxycycline from aqueous solutions. *Environ. Toxicol. Pharmacol.* 53, 121–132.
- Ren, X., Zeng, G., Tang, L., Wang, J., Wan, J., Liu, Y., Yu, J., Yi, H., Ye, S., Deng, R., 2018. Sorption, transport and biodegradation—an insight into bioavailability of persistent organic pollutants in soil. *Sci. Total Environ.* 610, 1154–1163.
- Rostamian, R., Behnejad, H., 2018. Insights into doxycycline adsorption onto graphene nanosheet: a combined quantum mechanics, thermodynamics, and kinetic study. *Environ. Sci. Pollut. Res.* 25, 2528–2537.
- Song, Q., Fang, Y., Liu, Z., Li, L., Wang, Y., Liang, J., Huang, Y., Lin, J., Hu, L., Zhang, J., 2017. The performance of porous hexagonal BN in high adsorption capacity towards antibiotics pollutants from aqueous solution. *Chem. Eng. J.* 325, 71–79.
- Senta, I., Matošić, M., Jakopović, H.K., Terzić, S., Čurko, J., Mijatović, I., Ahel, M., 2011. Removal of antimicrobials using advanced wastewater treatment. *J. Hazard Mater.* 192, 319–328.
- Stock, N., Biswas, S., 2011. Synthesis of metal-organic frameworks (MOFs): routes to various MOF topologies, morphologies, and composites. *Chem. Rev.* 112, 933–969.
- Si, X.L., Sun, L.X., Xu, F., Jiao, C.L., Li, F., Liu, S.S., Zhang, J., Song, L.F., Jiang, C.H., Wang, S., 2011. Improved hydrogen desorption properties of ammonia borane by Ni-modified metal-organic frameworks. *Int. J. Hydrogen Energy* 36, 6698–6704.
- Tang, W.W., Zeng, G.M., Gong, J.L., Liang, J., Xu, P., Zhang, C., Huang, B.B., 2014. Impact of humic/fulvic acid on the removal of heavy metals from aqueous solutions using nanomaterials: a review. *Sci. Total Environ.* 468, 1014–1027.
- Tang, L., Yu, J., Pang, Y., Zeng, G., Deng, Y., Wang, J., Ren, X., Ye, S., Peng, B., Feng, H., 2018. Sustainable efficient adsorbent: alkali-acid modified magnetic biochar derived from sewage sludge for aqueous organic contaminant removal. *Chem. Eng. J.* 336, 160–169.
- Tan, X., Liu, Y., Zeng, G., Wang, X., Hu, X., Gu, Y., Yang, Z., 2015. Application of biochar for the removal of pollutants from aqueous solutions. *Chemosphere* 125, 70–85.
- Tam, S.K., Dusseault, J., Polizu, S., Ménard, M., Hallé, J.-P., Yahia, L.H., 2005. Physicochemical model of alginate-poly-L-lysine microcapsules defined at the micrometric/nanometric scale using ATR-FTIR, XPS, and ToF-SIMS. *Biomaterials* 26, 6950–6961.
- Wang, P., Tang, L., Wei, X., Zeng, G., Zhou, Y., Deng, Y., Wang, J., Xie, Z., Fang, W., 2017. Synthesis and application of iron and zinc doped biochar for removal of p-nitrophenol in wastewater and assessment of the influence of co-existed Pb (II). *Appl. Surf. Sci.* 392, 391–401.
- Wu, H., Lai, C., Zeng, G., Liang, J., Chen, J., Xu, J., Dai, J., Li, X., Liu, J., Chen, M., 2017. The interactions of composting and biochar and their implications for soil amendment and pollution remediation: a review. *Crit. Rev. Biotechnol.* 37, 754–764.
- Wan, J., Zeng, G., Huang, D., Hu, L., Xu, P., Huang, C., Deng, R., Xue, W., Lai, C., Zhou, C., 2018. Rhamnolipid stabilized nano-chlorapatite: synthesis and enhancement effect on Pb-and Cd-immobilization in polluted sediment. *J. Hazard Mater.* 343, 332–339.
- Xu, H.Y., Yang, Z.H., Zeng, G.M., Luo, Y.L., Huang, J., Wang, L.K., Song, P.P., Mo, X., 2014. Investigation of pH evolution with Cr (VI) removal in electrocoagulation process: proposing a real-time control strategy. *Chem. Eng. J.* 239, 132–140.
- Xu, H.Y., Yang, Z.H., Luo, Y.L., Wang, P., Huang, J., Song, P.P., 2018. Study on a real-time control strategy to Cr(VI) removal with fluctuation of influent in Fe-electrocoagulation-Al-electroflotation reactor. *J. Electrochem. Soc.* 165, E366–E374.
- Xiong, W., Tong, J., Yang, Z., Zeng, G., Zhou, Y., Wang, D., Song, P., Xu, R., Zhang, C., Cheng, M., 2017. Adsorption of phosphate from aqueous solution using iron-zirconium modified activated carbon nanofiber: performance and mechanism. *J. Colloid Interface Sci.* 493, 17–23.
- Xiong, W., Zeng, Z., Li, X., Zeng, G., Xiao, R., Yang, Z., Zhou, Y., Zhang, C., Cheng, M., Hu, L., Zhou, C., Qin, L., Xu, R., Zhang, Y., 2018a. Multi-walled carbon nanotube/amino-functionalized MIL-53(Fe) composites: remarkable adsorptive removal of antibiotics from aqueous solutions. *Chemosphere* 210, 1061–1069.
- Xiong, W., Zeng, G., Yang, Z., Zhou, Y., Zhang, C., Cheng, M., Liu, Y., Hu, L., Wan, J., Zhou, C., 2018b. Adsorption of tetracycline antibiotics from aqueous solutions on nanocomposite multi-walled carbon nanotube functionalized MIL-53 (Fe) as new adsorbent. *Sci. Total Environ.* 627, 235–244.
- Xu, P., Zeng, G.M., Huang, D.L., Feng, C.L., Hu, S., Zhao, M.H., Lai, C., Wei, Z., Huang, C., Xie, G.X., 2012a. Use of iron oxide nanomaterials in wastewater treatment: a review. *Sci. Total Environ.* 424, 1–10.
- Xu, P., Zeng, G.M., Huang, D.L., Lai, C., Zhao, M.H., Wei, Z., Li, N.J., Huang, C., Xie, G.X., 2012b. Adsorption of Pb (II) by iron oxide nanoparticles immobilized Phanerochaete chrysosporium: equilibrium, kinetic, thermodynamic and mechanisms analysis. *Chem. Eng. J.* 203, 423–431.
- Yang, Z.H., Huang, J., Zeng, G.M., Ruan, M., Zhou, C.S., Li, L., Rong, Z.G., 2009. Optimization of flocculation conditions for kaolin suspension using the composite flocculant of MBFGA1 and PAC by response surface methodology. *Bioresour. Technol.* 100, 4233–4239.
- Zaidi, S., Chaabane, T., Sivasankar, V., Darchen, A., Maachi, R., Msagati, T., Prabhakaran, M., 2016. Performance efficiency of electro-coagulation coupled electro-flotation process (EC-EF) versus adsorption process in doxycycline removal from aqueous solutions. *Process. Saf. Environ.* 102, 450–461.
- Zhou, C., Lai, C., Xu, P., Zeng, G., Huang, D., Zhang, C., Cheng, M., Hu, L., Wan, J., Liu, Y., 2018. In situ grown AgI/Bi₁₂O₁₇Cl₂ heterojunction photocatalysts for visible light degradation of sulfamethazine: efficiency, pathway, and mechanism. *ACS Sustain. Chem. Eng.* 6, 4174–4184.
- Zhang, C., Lai, C., Zeng, G., Huang, D., Yang, C., Wang, Y., Zhou, Y., Cheng, M., 2016a. Efficacy of carbonaceous nanocomposites for sorbing ionizable antibiotic sulfamethazine from aqueous solution. *Water Res.* 95, 103–112.
- Zhang, Y., Zeng, G.M., Tang, L., Chen, J., Zhu, Y., He, X.X., He, Y., 2015. Electrochemical sensor based on electrodeposited graphene-Au modified electrode and nanoAu carrier amplified signal strategy for attomolar mercury detection. *Anal. Chem.* 87, 989–996.
- Zhang, X., Bai, B., Puma, G.L., Wang, H., Suo, Y., 2016b. Novel sea buckthorn bio-carbon SBC@β-FeOOH composites: efficient removal of doxycycline in aqueous solution in a fixed-bed through synergistic adsorption and heterogeneous Fenton-like reaction. *Chem. Eng. J.* 284, 698–707.
- Zhai, L., Bai, Z., Zhu, Y., Wang, B., Luo, W., 2018. Fabrication of chitosan microspheres for efficient adsorption of methyl orange. *Chin. J. Chem. Eng.* 26, 657–666.